Research Article

Gervais Mouthé Happi*, Klev Gaïtan Sikam, Mahmoud A. A. Ibrahim*, Liliane Clotilde Dzouemo, Guy-Paulin M. Kemayou, Praid Likane Keuteu, Peter A. Sidhom, Shaban R. M. Sayed, Mohamed-Elamir F. Hegazy, Jean Duplex Wansi*

Specialized compounds of four Cameroonian spices: Isolation, characterization, and *in silico* evaluation as prospective SARS-CoV-2 inhibitors

https://doi.org/10.1515/chem-2023-0203
received October 7, 2023; accepted May 24, 2024

Abstract: Since the emergency of coronavirus disease 2019, no specific drug has been developed within the fighting program against its spread. In Cameroon, it has been reported that the dish "yellow soup" can significantly curb the progress of the disease, while no chemical investigations have been done so far to support that conclusion. Chemical investigations of four selected spices of that dish led to the isolation of a total of 44 distinct pure compounds, which were identified using spectroscopic data. Furthermore, the docking scores of the isolated compounds were inspected by AutoDock4.2.6 software toward SARS-CoV-2 multi-targets involving main protease (M^{pro}), helicase, papain-like protease (PL^{pro}), and human angiotensin-converting enzyme 2 (ACE2). The most potent isolated compounds underwent molecular dynamics (MD) simulations over 100 ns. Stigmasterol demonstrated outstanding potency toward M^{pro} and PL^{pro} with $\Delta G_{binding}$ values of −35.6 and −36.6 kcal/mol, respectively, compared to nirmatrelvir. Nevertheless, 3β-taraxeryl acetate revealed good binding affinity against helicase and lupeol unveiled superior binding energy toward ACE2 compared to nirmatrelvir. Post-MD analyses manifested great steadiness of the isolated compounds within the binding pockets of SARS-CoV-2 targets throughout 100 ns MD simulations. Stigmasterol, 3β-taraxeryl acetate, and lupeol are recommended for further *in vivo*/*in vitro* tests toward SARS-CoV-2 multi-targets.

Keywords: phytochemical study, Cameroonian spices, COVID-19, MD simulations, docking computations

*** Corresponding author: Gervais Mouthé Happi,** Department of Chemistry, Higher Teacher Training College, The University of Bamenda, P.O Box 39, Bambili, Cameroon, e-mail: gervais20022003@yahoo.fr
*** Corresponding author: Mahmoud A. A. Ibrahim,** Computational Chemistry Laboratory, Chemistry Department, Faculty of Science, Minia University, Minia, 61519, Egypt; School of Health Sciences, University of KwaZulu-Natal, Westville Campus, Durban, 4000, South Africa, e-mail: m.ibrahim@compchem.net
*** Corresponding author: Jean Duplex Wansi,** Department of Chemistry, Faculty of Sciences, University of Douala, P.O. Box 24157, Douala, Cameroon, e-mail: jdwansi@yahoo.fr
Klev Gaïtan Sikam, Liliane Clotilde Dzouemo: Department of Chemistry, Faculty of Sciences, University of Douala, P.O. Box 24157, Douala, Cameroon
Guy-Paulin M. Kemayou: Department of Organic Chemistry, Faculty of Sciences, University of Yaounde I, P.O. Box 812, Yaounde, Cameroon
Praid Likane Keuteu: Department of Chemistry, Higher Teacher Training College, The University of Bamenda, P.O Box 39, Bambili, Cameroon
Peter A. Sidhom: Department of Pharmaceutical Chemistry, Faculty of Pharmacy, Tanta University, Tanta, 31527, Egypt
Shaban R. M. Sayed: Department of Botany and Microbiology, College of Science, King Saud University, P.O. Box 2455, Riyadh, 11451, Saudi Arabia
Mohamed-Elamir F. Hegazy: Department of Pharmaceutical Biology, Institute of Pharmaceutical and Biomedical Sciences, Johannes Gutenberg University, Staudinger Weg 5, 55128 Mainz, Germany

1 Introduction

A medical emergency has been brought on by the severe acute respiratory syndrome coronavirus 2 (SARS-CoV-2), which was initially discovered in December 2019 in Wuhan, China. Until now, coronavirus disease 2019 (COVID-19) has been responsible for almost 7 million deaths and was classified as an international pandemic by the World Health Organization [1]. Numerous virus variants, such as Alpha, Delta, or Omicron, with greater virulence to humans and mutations, have been recorded in several regions worldwide. These variants increase the concern about the virus's resistance to human bodies and therefore keep urgent the search for potent molecules that can serve as leads to control the virus spread beyond the prescription of vaccines [2]. During the pandemic, several debates on possible curative modes of the disease and numerous suggestions of non-conventional or pharmaceutical medicines have been widely divulgated

through several media. Amongst them, Oben and co-workers reported in 2020 that the Cameroonian functional food 'star yellow' might be used to prohibit the prevalence of COVID-19. The authors indicated that the 'star yellow' has been prepared by adding *Cucumeropsis mannii* and *Allium sativum* to the common "yellow soup," which contains spices displaying well-known antibacterial/antiviral activities [3]. Notably, no chemical and computational investigations have been performed so far to identify the chemical constituents of those main spices and their identification as potent leads in the control of the disease. Since the outbreak of COVID-19 infection, a recent study demonstrated the efficiency of herbal extracts and spices to inhibit SARS-CoV-2 and prohibit this infection [4]. In seeking inhibitors to combat SARS-CoV-2 reproduction, four spices were investigated. These spices commonly used in the Cameroonian dish "yellow soup", responsible for its taste, namely *Tetrapleura tetraptera* (Schum. & Thonn.) (Fabaceae), *Zanthoxylum gilletii* (De Wild.) P.G. Waterman (Rutaceae), *Afrostyrax lepidophyllus* (Mildbr.) (Huaceae), and *Piper guineense* (Schumach. & Thonn.) (Piperaceae). Therefore, this work was set out to assess the binding affinities of the 44 isolated compounds against SARS-CoV-2 multi-targets by AutoDock4.2.6 software. Based on the predicted docking scores, the most promising isolated molecules subsequently underwent molecular dynamics (MD) simulations throughout 100 ns. The steadiness and binding affinities of the investigated compounds were inspected during the 100 ns MD simulations. These outcomes shine new light on the significance of the identified molecules, which could be investigated *in vivo*/*in vitro* to combat the worldwide impendence of COVID-19 infection.

2 Materials and methods

2.1 General instrumentation

The chemical investigations of the plant extracts, including the isolation of the compounds and their structural identification, have been done using similar instruments as described in our recently published work [5]. More specifics linked to general instrumentation can be obtained from the supplementary material.

2.2 Plant material

The four spices investigated during this study have been harvested or purchased in several localities of Cameroon. For instance, the plant material of *Tetrapleura tetraptera* (Schum. & Thonn.) Taub. (roots and stem bark) was harvested in March 2020 at Bafang (GPS coordinates: longitude 10°11′28″E, latitude 5°09′32″N, elevation: 1,280 m). The stem bark of *Zanthoxylum gilletii* (De Wild.) P.G. Waterman was harvested at Bana-Tentcheu (GPS coordinates: longitude 10°17′41″ E, latitude 5°07′57″N, elevation: 1,412 m), West region, Cameroon, in April 2021. However, the seeds of *Afrostyrax lepidophyllus* Mildbr. and *Piper guineense* Schumach. & Thonn. were purchased in the Mokolo market (GPS coordinates: latitude 3°52′ 28″N, longitude 11°30′6″E, elevation: 192 m) in June 2021. Mr. Victor Nana, a botanist, identified the plants by comparing them to plant material included in the database of the National Herbarium of Cameroon. Specimens for each plant were kept under the voucher numbers 31310 HNC, 38960 HNC, 39020 HNC, and 43129 HNC for *T. tetraptera*, *Z. gilletii*, *A. lepidophyllus*, and *piper guineense*, respectively.

2.3 Extraction and isolation

Forty-four unique chemicals were isolated as a result of the four plants that were collected being chemically examined. The protocol for their segregation can be obtained from the supplementary data related to this manuscript.

2.4 Computational methodology

2.4.1 SARS-CoV-2 multi-targets preparation

The crystal structures of main protease (M^{pro}), papain-like protease (PL^{pro}), helicase, and angiotensin-converting enzyme 2 (ACE2) (PDB IDs: 6LU7 [6], 6W9C [7], 5RMM [8], and 6M0J [9], respectively, were downloaded and used as templates for all *in silico* computations. For the preparation purpose, all ligands, water, and ions were extracted. To build the missing residues, Modeller software was used [10]. The protonation states of the inspected targets were also assigned using the H++ server [11]. All missing hydrogens were added.

2.4.2 Ligand preparation

In SDF format, the 44 chemical structures were obtained from the PubChem database (https://pubchem.ncbi.nlm.nih.gov). The three-dimensional structures of the isolated compounds were generated utilizing Omega2 software [12,13]. Utilizing the MMFF94S inside the SZYBKI software, the created structures were optimized [14,15]. The evaluated compounds' atomic charges were assigned using the Gasteiger method [16].

2.4.3 Docking computations

All docking computations were conducted by AutoDock4.2.6 software [17]. The SARS-CoV-2 multi-targets were prepared as described in Ref. [18–20]. The *GA* (genetic algorithm) was adjusted to 250. The *eval* (maximum number of energy evaluations) was set to 25,000,000. Other docking parameters were kept at their default values. The size of the grid box was 60 Å × 60 Å × 60 Å. The grid box was positioned at the center of SARS-CoV-2 multi-targets. A grid spacing of 0.375 Å was used. The grid maps were generated using the AutoGrid program.

2.4.4 MD simulations

All MD simulations were carried out using the AMBER16 software [21]. The applied MD simulations' technical details are characterized elsewhere [22,23]. In an abridged, the isolated compounds were parameterized using the General AMBER force field (GAFF2) [24]. The studied targets were characterized utilizing AMBER force field 14SB [25]. Using the Gaussian09 software, the isolated compounds were optimized at the HF/6-31G* level [26]. Restrained electrostatic potential (RESP) approach was employed to assign the atomic charges of the isolated compounds [27]. For preparation purposes, all complexes were centered in an octahedron box of the TIP3P water model. To make the complexes electrically neutral, the Na+/Cl− counterions were inserted. Energy minimization for 5,000 cycles was employed to remove any steric clashes. After that, all minimized systems were smoothly annealed up to 310 K over 50 ps. All heated systems were then equilibrated for 10 ns. Ultimately, the production runs were executed for 100 ns. All MD simulations were executed by the GPU-accelerated pmemd.cuda version of the AMBER16 software package on the CompChem hybrid GPU/CPU cluster (hpc.compchem.net). All molecular interactions were visualized utilizing BIOVIA Materials Studio [28].

2.4.5 Binding energy evaluation

The binding energy ($\Delta G_{\text{binding}}$) between the isolated compounds and SARS-CoV-2 multi-targets was estimated by employing the Molecular Mechanics-Generalized Born Surface Area (MM-GBSA) approach [29]. The calculation formula is as follows:

$$\Delta G_{\text{binding}} = G_{\text{Complex}} - (G_{\text{Inhibitor}} + G_{\text{Receptor}}),$$

where the G (energy factor) is computed from:

$$G = G_{\text{SA}} + G_{\text{GB}} + E_{\text{vdw}} + E_{\text{ele}},$$

G_{GB} refers to electrostatic solvation-free energy. G_{SA} is the nonpolar solvation-free energy. E_{ele} is the electrostatic energy. E_{vdw} is the van der Waals energy. A single-frame method was employed, in which the coordinates of each inhibitor, receptor, and inhibitor–receptor were obtained from a single frame. The entropy contribution (S) is ignored because of the greatest *in-silico* costs and time [30,31].

3 Results and discussion

3.1 Phytochemical investigation

The phytochemical investigations carried out in this work consisted of the search for chemical constituents of four spices commonly used for cooking the Cameroonian dish "yellow soup" which was claimed a functional food capable of controlling the pathology of the SARS-CoV-2 [3]. Their chemical investigations led to the isolation of 44 different molecules; some isolated from more than one spice. The results indicated that 16 specialized compounds (**1**–**16**) were separated from the bark and roots of *Tetrapleura tetraptera* (Figure 1) [32]. Nine compounds (**11**, **16**, **17**–**23**) were separated from the seeds of *Afrostyrax lepidophyllus* (Figure 2). The chemical analysis of the methanol extract of *Zanthoxylum gilletii* bark resulted in the separation and characterization of thirteen compounds (**24**–**36**) (Figure 3). Nine compounds (**30**, **37**–**44**) were obtained from the seeds of *Piper guineense* (Figure 4).

Taken together, the 44 distinct molecules have been characterized according to their spectroscopic data (^{1}H, 2D-NMR, and ^{13}C) data, and these data were compared with those reported in the literature. Therefore, the isolated compounds were identified as rhusopolyphenol F (**1**) [33], butein (**2**) [34], lupeol (**3**) [35,36], lupenone (**4**) [37], betulin (**5**) [38], betulinic acid (**6**) [39], maslinic acid (**7**), arjungenin (**8**) [40], aridanin (**9**) [41], hederagenin-3-*O*-α-L-arabinopyranoside (**10**) [42], ursolic acid (**11**) [34], tormentic acid (**12**) [43], 3β-taraxeryl acetate (**13**) [44], rhaponticin (**14**) [35], stigmasterol (**15**), stigmasterol-3-*O*-β-D-glucopyranoside (**16**) [45], β-amyryl acetate (**17**) [46], palmitic acid (**18**) [47], tripalmitin (**19**) [48], sucrose (**20**) [49], monomethyl citrate (**21**) [50], 1,3-dioxepane (**22**) [51], sitosterol-3-*O*-β-D-glucopyraonosyl-*O*-6-palmitate (**23**) [46], 5-hydroxynoracronycine (**24**) [46], decarine (**25**) [52], oxychelerythrine (**26**) [53], arnottianamide (**27**) [54], *trans*-fagaramide (**28**) [55], *cis*-fagaramide (**29**) [56], sesamin (**30**) [57], scoparone (**31**) [58], scopoletin (**32**) [46], fridelin (**33**) [59], erythrodiol-3-

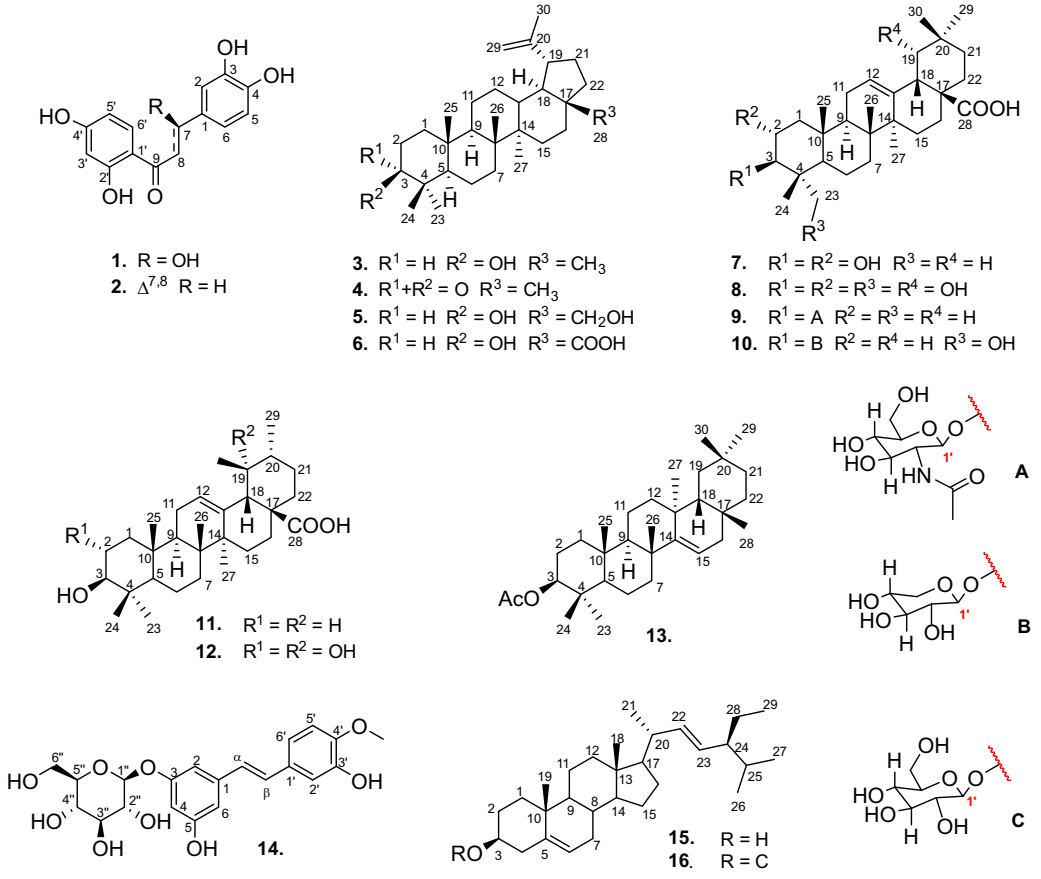

Figure 1: Chemical structures of compounds (**1**–**16**) isolated from *T. tetraptera.*

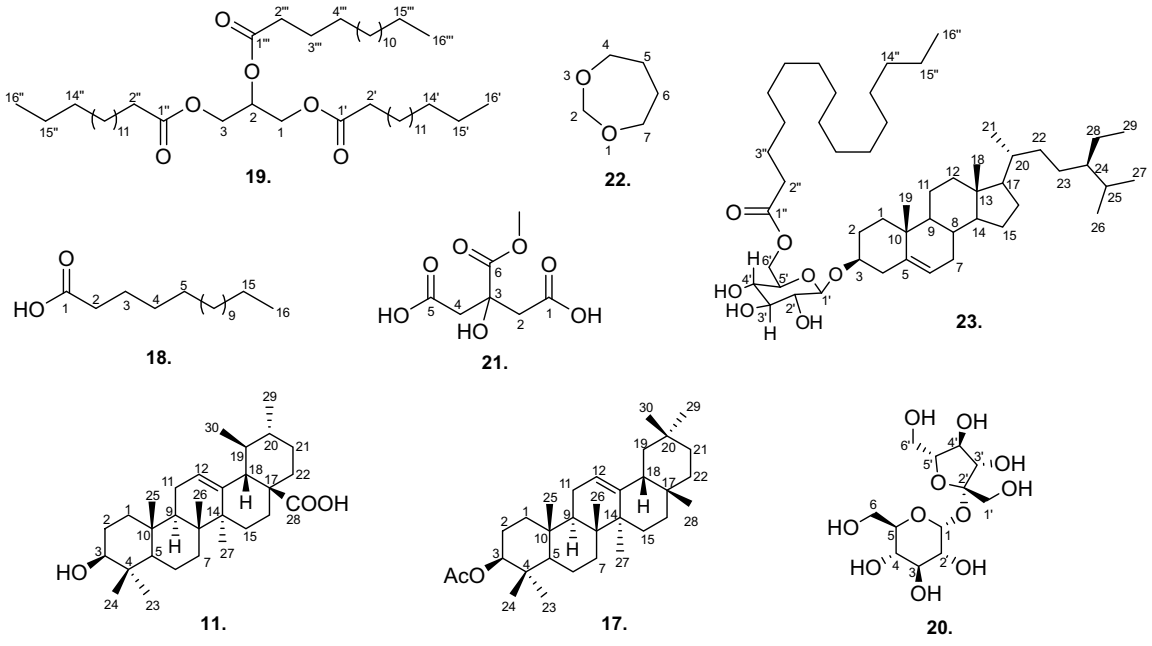

Figure 2: Chemical structures of some compounds (**11**, **17**–**23**) isolated from *A. lepidophyllus.*

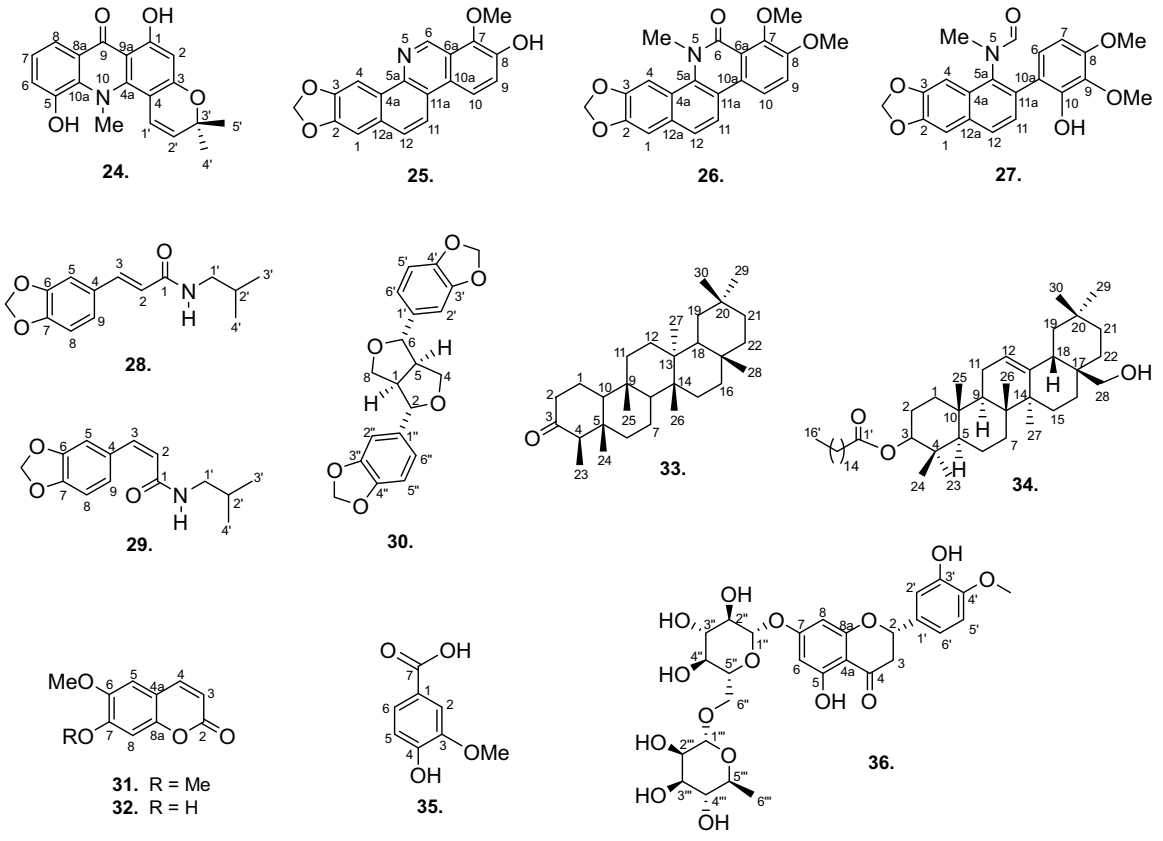

Figure 3: Chemical structures of some compounds (**24**–**36**) isolated from *Z. gilletii.*

O-palmitate (**34**) [60], vanillic acid (**35**) [55], hesperidin (**36**) [61], piperine (**37**) [62], piperic acid (**38**) [63], wisanine (**39**) [64], okolasine (**40**) [64,65], dihydrowisanidine (**41**) [64], guineensine (**42**) [64], tyrosyl palmitate (**43**) [66], and palmityl ferulate (**44**) [67].

3.2 Spectroscopic data of isolated molecules

Spectroscopic data of the isolated molecules (**1**–**44**) are found in the supplementary material associated with this article (**Figures S1–S83**).

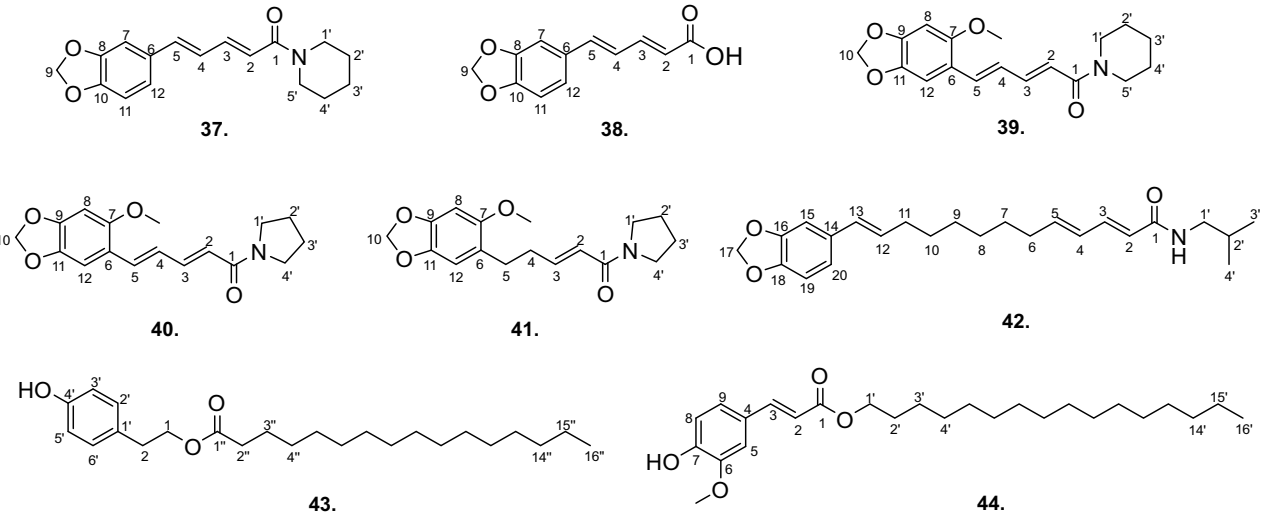

Figure 4: Chemical structures of some compounds (**37**–**44**) isolated from *P. guineense.*

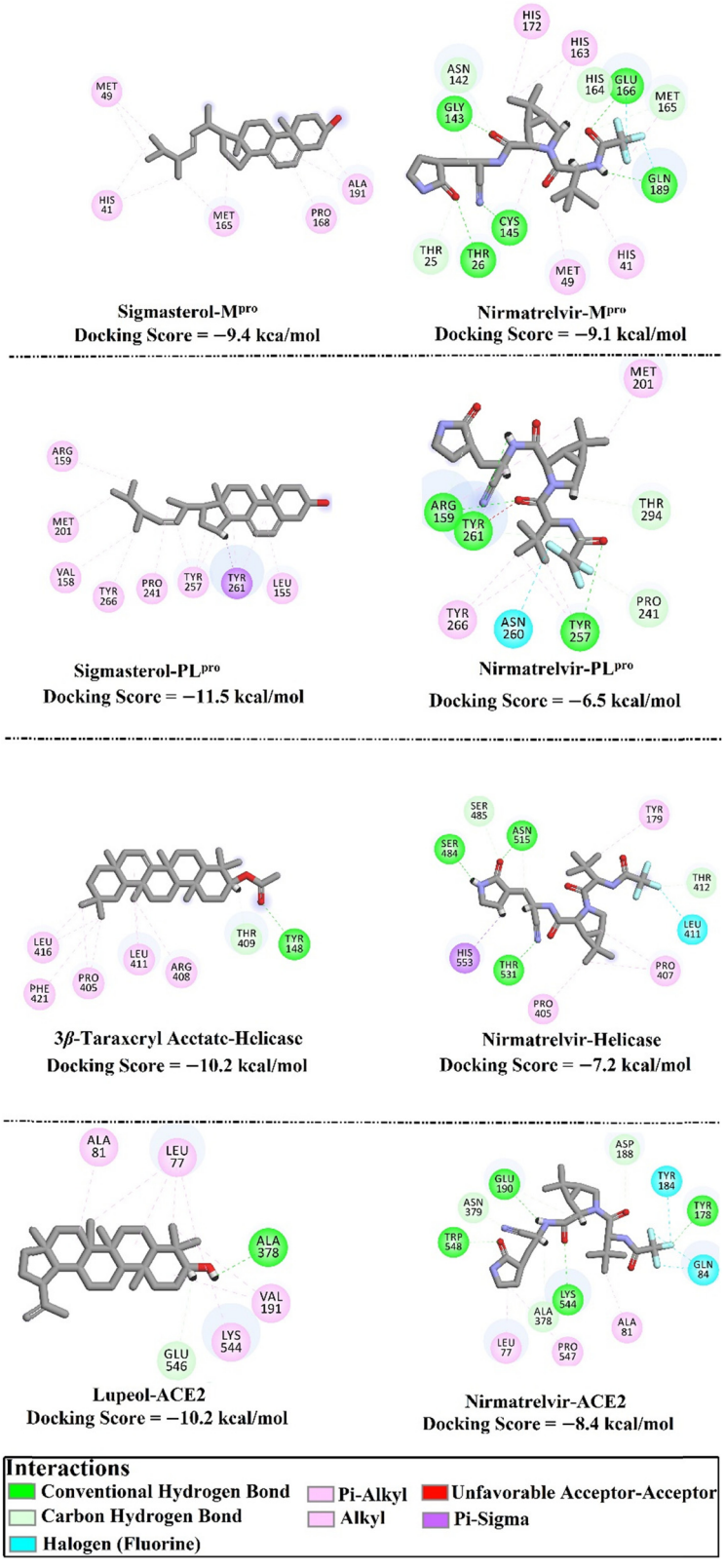

Figure 5: 2D molecular interactions of the most potent compounds with essential residues of viral and human targets, namely, M^{pro}, PL^{pro}, helicase, and ACE2.

Table 1: Estimated binding energies for nirmatrelvir and the most potent compounds complexed with viral and human targets during 100 ns MD simulations

Compound name	MM-GBSA-binding energy (kcal/mol)			
	M^{pro}	PL^{pro}	Helicase	ACE2
Nirmatrelvir	−32.6	−28.6	−42.7	−31.4
Stigmasterol	−35.6	−36.6	–[a]	–[a]
3β-Taraxeryl acetate	–[a]	–[a]	−43.5	–[a]
Lupeol	–[a]	–[a]	–[a]	−39.1

[a]No binding energy was calculated.

3.3 *In silico* drug discovery

3.3.1 Molecular docking

To predict the binding scores and poses of 44 isolated molecules toward SARS-CoV-2 multi-targets, the molecular docking technique was used. The isolated molecules were prepared and docked into the binding pockets of the M^{pro}, PL^{pro}, helicase, and ACE2 with the assistance of AutoDock4.2.6 software. Docking scores and two-dimensional (2D) chemical structures are gathered in Table S1. From Table S1, the investigated compounds with M^{pro}, PL^{pro}, helicase, and ACE2 demonstrated a broad range of binding scores with values ranging from −4.1 to −9.4, from −3.7 to −11.5, from −2.7 to −10.2, and from −3.8 to −10.2 kcal/mol, respectively. Stigmasterol, unsaturated phytosterol obtained from plant fats or oils, revealed promising binding scores toward M^{pro} and PL^{pro} with values of −9.4 and −11.5 kcal/mol, respectively (Table S1 and Figure 5). The outstanding potentiality of stigmasterol as M^{pro} and PL^{pro} inhibitor is ascribed to its capability of exhibiting hydrophobic, pi-based, and vdW (van der Waals) interactions with the essential residues within the binding pockets of M^{pro} and PL^{pro} (Figure 5). Notwithstanding, 3β-taraxeryl acetate unveiled surpassed potentiality docking score against helicase enzyme with a value of −10.2 kcal/mol (Figure 5).

Specifically, 3β-taraxeryl acetate showed an H-bond with TYR148 residue (2.63 Å) within the binding pocket of helicase (Table S1 and Figure 5). Lupeol, a pentacyclic triterpenoid, manifested a good docking score toward ACE2 protein with a value of −10.2 kcal/mol. Lupeol formed an H bond with ALA378 residue (2.11 Å) and a carbon-H bond with GLU546 residue. Lupeol also exhibited alkyl interactions with ALA81, LEU77, VAL191, and LYS544 residues (Table S1 and Figure 5).

Nirmatrelvir, whose role as an orally active protease inhibitor developed by Pfizer, was utilized as a reference drug because the U.S. Food and Drug Administration allowed an emergency utilize authorization to nirmatrelvir/ritonavir (Paxlovid®) [68,69]. Nirmatrelvir displayed good docking scores with values of −9.1, −6.5, −7.2, and −8.4 kcal/mol toward M^{pro}, PL^{pro}, helicase, and ACE2, respectively (Table S1 and Figure 5). Nirmatrelvir exhibited five H bonds with THR26, GLY143, CYS145, GLU166, and GLN189 residues inside the binding pocket of the M^{pro} with bond lengths of 2.57, 1.71, 2.26, 1.83, and 2.51 Å, respectively (Figure 5). Nirmatrelvir formed three H bonds with ARG159 (2.30 Å), TYR257 (3.11 Å), and TYR261 (2.32 Å); SER484 (1.81 Å), ASN515 (2.18 Å), and THR531 (2.28 Å); and LYS544 (2.25 Å), TRP548 (2.08 Å), and GLU190 (2.76 Å) within the binding pocket of PL^{pro}, helicase, and ACE2, respectively (Figure 5). A docking comparison of nirmatrelvir with stigmasterol, 3β-taraxeryl acetate, and lupeol disclosed docking scores proposing the prospectivity of the three isolated compounds as inhibitors of SARS-CoV-2 multi-targets.

3.3.2 MD simulations

The dynamic nature of the receptor–inhibitor complex has been vastly investigated using MD simulations for examining conformational variances, receptor–inhibitor steadiness, and internal motions [70,71]. Stigmasterol complexed with M^{pro} and PL^{pro}, 3β-taraxeryl acetate-helicase, and lupeol-ACE2 complexes were further investigated by MD simulations during 100 ns. According to gathered trajectories throughout the production phase of 100 ns, the binding energies ($\Delta G_{binding}$) were evaluated utilizing the

Table 2: The evaluated binding energy ($\Delta G_{binding}$) and the corresponding individual energy terms for stigmasterol-M^{pro}, stigmasterol-PL^{pro}, 3β-taraxeryl acetate-helicase, and lupeol-ACE2 complexes throughout 100 ns MD simulations

Compound name	MM-GBSA binding energy (kcal/mol)						
	ΔE_{vdw}	ΔE_{ele}	ΔE_{GB}	ΔE_{SUR}	ΔG_{gas}	ΔG_{solv}	$\Delta G_{binding}$
Stigmasterol-M^{pro}	−43.8	−2.6	15. 6	−4.7	−46.4	10.8	−35.6
Stigmasterol-PL^{pro}	−46.0	−1.5	16.3	−5.4	−47.5	10.9	−36.6
3β-Taraxeryl acetate-helicase	−57.5	−1.9	22.4	−6.4	−59.2	16.0	−43.5
Lupeol-ACE2	−50.0	−10.2	26. 6	−5.8	−60.2	20.8	−39.4

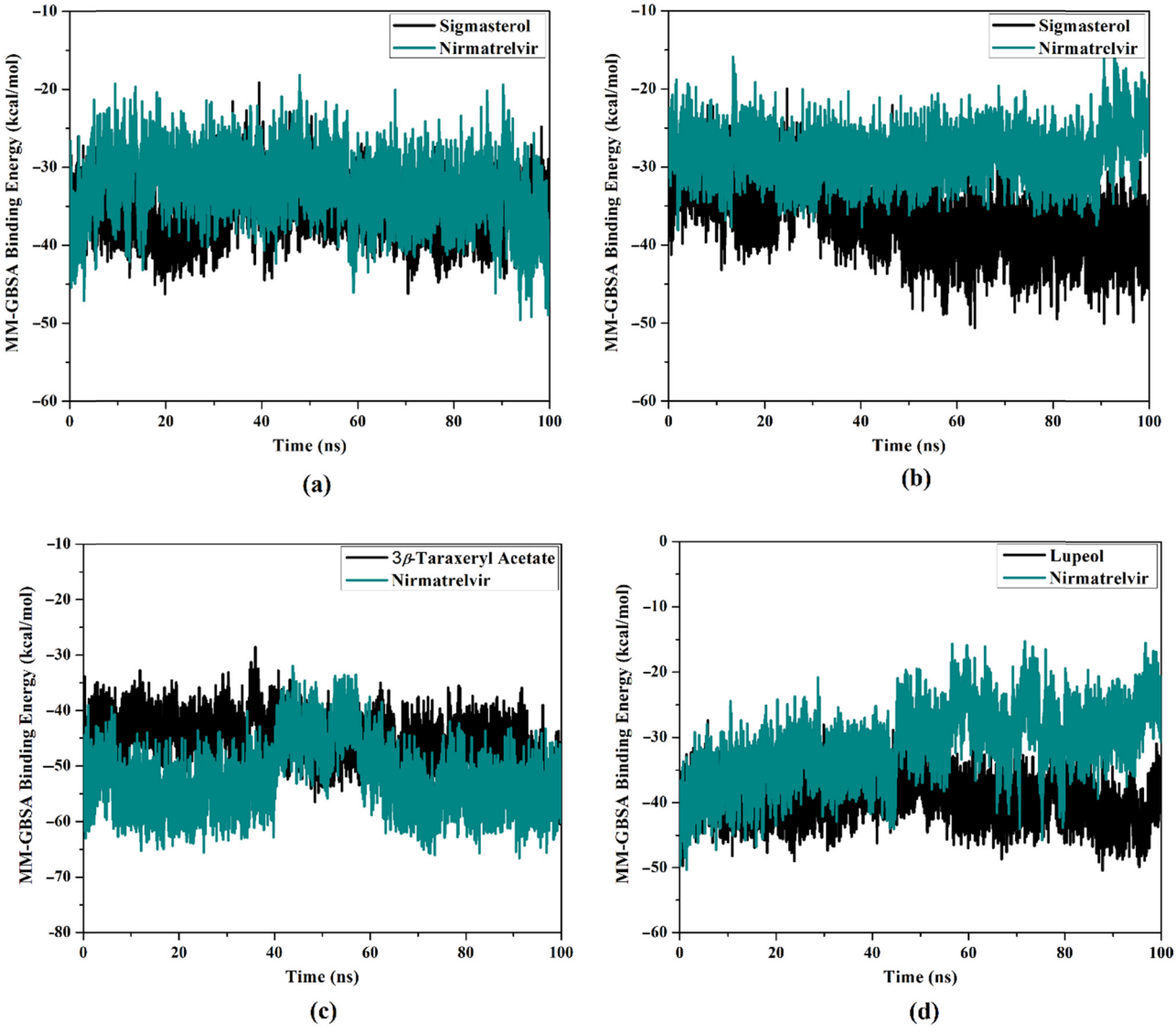

Figure 6: Computed binding energies per trajectory for investigated compounds (in black) and nirmatrelvir (dark cyan) complexed with SARS-CoV-2 and human targets over 100 ns MD simulations. (a) M^{pro}, (b) PL^{pro}, (c) helicase, (d) ACE2.

MM-GBSA approach and are compiled in Table 1. Stigmasterol complexed with M^{pro} and PL^{pro} demonstrated promising $\Delta G_{binding}$ with values of −35.6 and −36.6 kcal/mol, respectively (Table 1). However, 3β-taraxeryl acetate with helicase manifested good $\Delta G_{binding}$ with a value of −43.5 kcal/mol (Table 1). Lupeol complexed with ACE2 revealed outstanding $\Delta G_{binding}$ with a value of −39.1 kcal/mol (Table 1). Compared to nirmatrelvir (calc. −32.6, −28.6, −42.7, and −31.4 kcal/mol toward M^{pro}, PL^{pro}, helicase, and ACE2, respectively), the binding energy of nirmatrelvir was similar to that of 3β-taraxeryl acetate complexed with helicase, while stigmasterol complexed with M^{pro} and PL^{pro} and lupeol complexed with ACE2, in fact, disclosed a considerably greater binding affinity.

To explore the nature of the predominant interactions, the computed $\Delta G_{binding}$ and the energy components of the most promising compounds complexed with SARS-CoV-2 and human targets estimated by the MM-GBSA approach are listed in Table 2. Binding energy was dominated by van der Waals (E_{vdw}) forces for stigmasterol complexed with M^{pro} and PL^{pro}, 3β-taraxeryl acetate-helicase, and lupeol-ACE2 complexes with average values of −43.8, −46.0, −57.5, and −50.0 kcal/mol, respectively. Electrostatic (E_{ele}) forces provided favorable contributions in the binding energy of stigmasterol complexed with M^{pro} and PL^{pro}, 3β-taraxeryl acetate-helicase, and lupeol-ACE2 complexes with average values of −2.6, −1.5, −1.9, and −10.2 kcal/mol, respectively

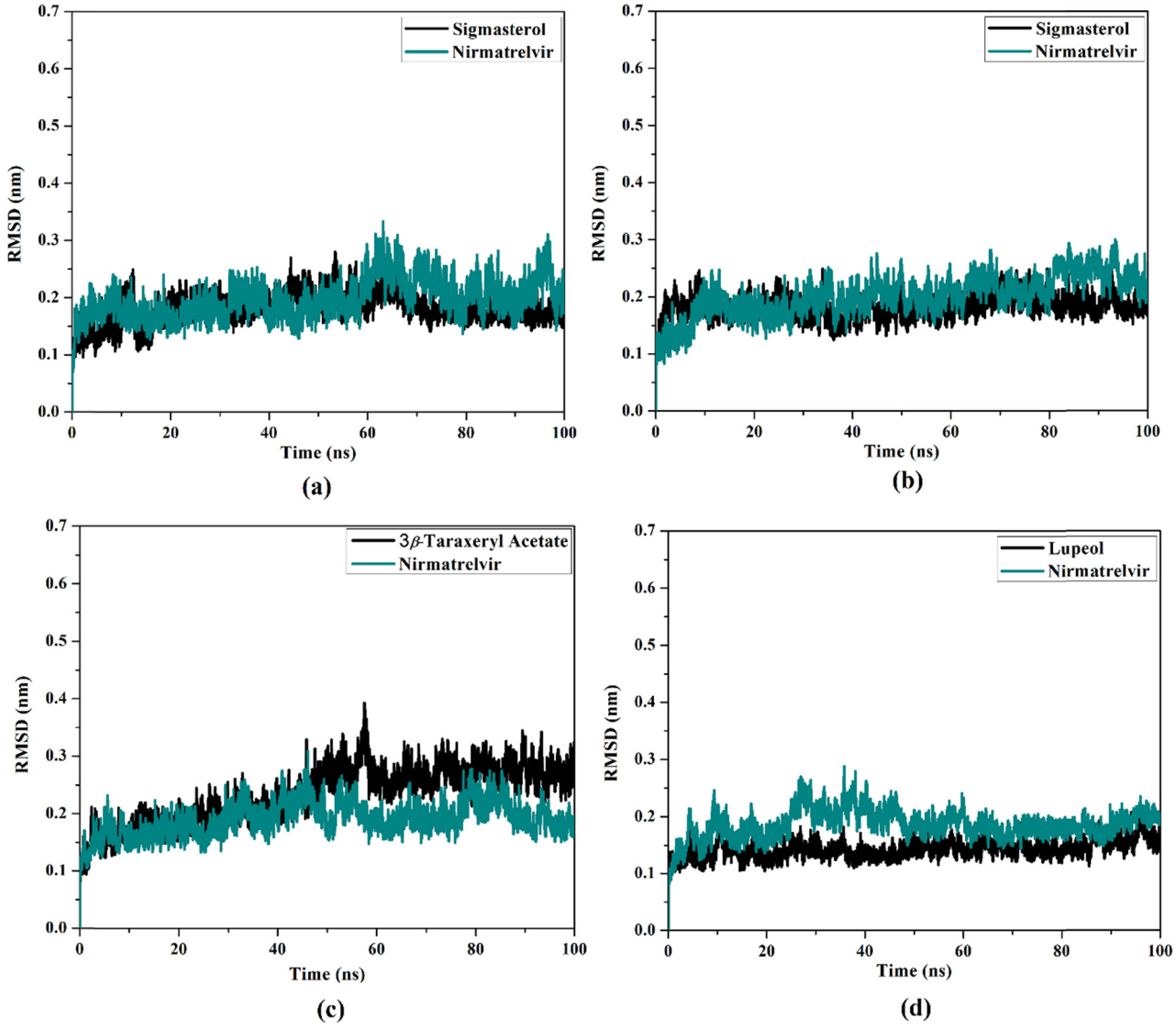

Figure 7: RMSD of the backbone relative to the initial complexes over 100 ns MD course for investigated compounds (in black) and nirmatrelvir (dark cyan) complexed with SARS-CoV-2 and human targets. (a) M^{pro}, (b) PL^{pro}, (c) helicase, (d) ACE2.

(Table 2). Together, these results provide quantitative data on stigmasterol, 3β-taraxeryl acetate, and lupeol as anti-COVID-19 drug candidates.

3.3.3 Post-MD analyses

While docking computations and MD simulations, followed by $\Delta G_{binding}$ computations, demonstrated the potentiality of stigmasterol, 3β-taraxeryl acetate, and lupeol as anti-COVID-19 drug candidates, further post-MD analyses would be demanded to unveil the energetical and structural steadiness for inhibitor-receptor interactions. These analyses involved binding energy per trajectory and root-mean-square deviation (RMSD).

3.3.3.1 Binding energy per trajectory

Binding energy per trajectory for stigmasterol-M^{pro}, stigmasterol-PL^{pro}, 3β-taraxeryl acetate-helicase, and lupeol-ACE2 complexes were estimated and compared to nirmatrelvir throughout 100 ns MD course (Figure 6). From Figure 6, comprehensive steadiness for stigmasterol-M^{pro}, stigmasterol-PL^{pro}, 3β-taraxeryl acetate-helicase, and lupeol-ACE2 complexes was noticed over MD simulations with $\Delta G_{binding}$ values of −35.6, −36.6, −43.5, and −39.4 kcal/mol, respectively. Compared to stigmasterol-M^{pro}, stigmasterol-PL^{pro}, 3β-taraxeryl acetate-helicase, and lupeol-ACE2 complexes, nirmatrelvir demonstrated good stabilities toward M^{pro}, PL^{pro}, helicase, and ACE2 with $\Delta G_{binding}$ values of −32.6, −28.6, −42.7, and −31.4 kcal/mol, respectively. These findings

indicated the great constancy of the inspected compounds complexed with SARS-CoV-2 and human targets.

3.3.3.2 RMSD

To check the conformational change of the stigmasterol-M^{pro}, stigmasterol-PL^{pro}, 3β-taraxeryl acetate-helicase, and lupeol-ACE2 complexes during the MD course, the RMSD of the backbone atoms relative to their respective starting positions was measured (Figure 7). Interestingly, the estimated RMSD for the inspected complexes remained below 0.35 nm over the simulated time. The stigmasterol-M^{pro}, stigmasterol-PL^{pro}, 3β-taraxeryl acetate-helicase, and lupeol-ACE2 complexes reached the equilibration phase in the first 15 ns MD simulations and proceeded to stationary state till the end of the simulations. Overall, these findings indicated that these compounds are capable of binding steadily to SARS-CoV-2 and human targets without influencing the comprehensive topology of the investigated targets.

4 Conclusion

The chemical investigations of four spices used for the preparation of the Cameroonian functional food "yellow soup" claimed to control the spread of COVID-19 led to the extraction of forty-four different compounds belonging to several classes of natural products. Utilizing AutoDock4.2.6 software, the isolated compounds were inspected as putative competitive inhibitors of SARS-CoV-2 M^{pro}, helicase, PL^{pro}, and ACE2. Docking computations unveiled the promising docking scores of stigmasterol with M^{pro} and PL^{pro}, 3β-taraxeryl acetate with helicase, and lupeol with ACE2 with values of −9.4, −11.5, −10.2, and −10.2 kcal/mol, respectively. These compounds, when submitted to MD simulations, manifested auspicious binding energies toward M^{pro}, PL^{pro}, helicase, and ACE2 (calc. −35.6, −36.6, −43.5, and −39.4 kcal/mol, respectively). Energetical and structural studies revealed high steadiness of inhibitors in complex with SARS-CoV-2 and human targets. These findings revealed three compounds isolated from Cameroon's promising natural products, stigmasterol, 3β-taraxeryl acetate, and lupeol, as prospective inhibitors of SARS-CoV-2 and human targets. The Cameroonian dish "yellow soup" can be classified as a functional food that might help to control the curve of SARS-CoV-2 infections through its bioactive chemical constituents. However, additional chemical, pharmacological, and pharmacokinetics studies might be important to provide further insights into its proper formulation.

Acknowledgements: The phytochemical works of this publication have been eased by Research Allowances to G.M.H. as well as the laboratory equipment support from the Alexander von Humboldt Foundation to J.W.D. M.A.A.I. thanks the Center for High-Performance Computing (CHPC, www.chpc.ac.za), Cape Town, South Africa, for providing computational resources. The authors extend their appreciation to the Researchers Supporting Project number (RSPD2024R743), King Saud University, Riyadh, Saudi Arabia, for funding this work.

Funding information: Authors state no funding involved.

Author contributions: G.M.H. – conceptualization, funding acquisition, project administration, resources, supervision, writing – review and editing; K.G.S. – data curation, formal analysis, investigation, writing – original draft; M.A.A.I. – resources, software, writing – review and editing; L.C.D. – data curation, formal analysis, investigation, writing – original draft; G.-P.M.K. – formal analysis, validation, writing – review and editing; P.L.K. – formal analysis, validation, writing – review and editing; P.A.S. – visualization, writing – review and editing; S.R.M.S. – funding acquisition, resources, writing – review and editing; M.-E.F.H. – visualization, writing – review and editing; and J.D.W. – conceptualization, methodology, project administration, supervision, writing – review and editing. All authors have read and agreed to the published version of the manuscript.

Conflict of interest: Authors state no conflict of interest.

Ethical approval: The conducted research is not related to either human or animal use.

Data availability statement: All data generated or analyzed during this study are included in this published article (and its supplementary information files).

References

[1] World Health Organization. WHO director-general's remarks at the media briefing on 2019-nCoV on 11 February 2020 [cited 2020 Apr 2]. https://www.who.int/dg/speeches/detail/who-director-general-s-remarks-at-the-media-briefing-on-2019-ncov-on-11-february-2020.

[2] Chapman RL, Andurkar SV. A review of natural products, their effects on SARS-CoV-2 and their utility as lead compounds in the discovery of drugs for the treatment of COVID-19. Med Chem Res. 2022;31:40–51.

[3] Oben J, Bigoga J, Takuissu G, Teta I, Leke R. The acceptability of 'Star Yellow,' a Cameroonian functional food that could curb the spread of the COVID-19 via feces. J Funct Food Health Dis. 2020;10:324–9.

[4] Ibrahim MAA, Abdelrahman AHM, Hussien TA, Badr EAA, Mohamed TA, El-Seedi HR, et al. *In silico* drug discovery of major metabolites from spices as SARS-CoV-2 main protease inhibitors. Comput Biol Med. 2020;126:104046.
[5] Happi GM, Dzouemo LC, Kemayou GPM, Meikeu LZ, Sikam KG, Yimtchui MT, et al. Antiplasmodial compounds from Urera gravenreuthii (Urticaceae), their structure-activity relationship and chemotaxonomic significance. South Afr J Bot. 2023;157:201–8.
[6] Jin Z, Du X, Xu Y, Deng Y, Liu M, Zhao Y, et al. Structure of M(pro) from SARS-CoV-2 and discovery of its inhibitors. Nature. 2020;582:289–93.
[7] Gao X, Qin B, Chen P, Zhu K, Hou P, Wojdyla JA, et al. Crystal structure of SARS-CoV-2 papain-like protease. Acta Pharm Sin B. 2021;11:237–45.
[8] Newman JA, Douangamath A, Yadzani S, Yosaatmadja Y, Aimon A, Brandao-Neto J, et al. Structure, mechanism and crystallographic fragment screening of the SARS-CoV-2 NSP13 helicase. Nat Commun. 2021;12:4848.
[9] Lan J, Ge J, Yu J, Shan S, Zhou H, Fan S, et al. Structure of the SARS-CoV-2 spike receptor-binding domain bound to the ACE2 receptor. Nature. 2020;581:215–20.
[10] Marti-Renom MA, Stuart AC, Fiser A, Sanchez R, Melo F, Sali A. Comparative protein structure modeling of genes and genomes. Annu Rev Biophys Biomol Struct. 2000;29:291–325.
[11] Gordon JC, Myers JB, Folta T, Shoja V, Heath LS, Onufriev A. H++: a server for estimating pKas and adding missing hydrogens to macromolecules. Nucleic Acids Res. 2005;33:W368–71.
[12] OMEGA 2.5.1.4, 2.5.1.4. OpenEye Scientific Software: Santa Fe, NM, USA; 2013.
[13] Hawkins PC, Skillman AG, Warren GL, Ellingson BA, Stahl MT. Conformer generation with OMEGA: algorithm and validation using high quality structures from the Protein Databank and Cambridge Structural Database. J Chem Inf Model. 2010;50:572–84.
[14] Halgren TA. MMFF VI. MMFF94s option for energy minimization studies. J Comput Chem. 1999;20:720–9.
[15] SZYBKI 1.9.0.3. OpenEye Scientific Software: Santa Fe, NM, USA; 2016.
[16] Gasteiger J, Marsili M. Iterative partial equalization of orbital electronegativity – a rapid access to atomic charges. Tetrahedron. 1980;36:3219–28.
[17] Morris GM, Huey R, Lindstrom W, Sanner MF, Belew RK, Goodsell DS, et al. AutoDock4 and AutoDockTools4: Automated docking with selective receptor flexibility. J Comput Chem. 2009;30:2785–91.
[18] Ibrahim MAA, Badr EAA, Abdelrahman AHM, Almansour NM, Mekhemer GAH, Shawky AM, et al. *In silico* targeting human multidrug transporter ABCG2 in breast cancer: Database screening, molecular docking, and molecular dynamics study. Mol Inform. 2022;41:e2060039.
[19] Ibrahim MAA, Abdelrahman AHM, Jaragh-Alhadad LA, Atia MAM, Alzahrani OR, Ahmed MN, et al. Exploring toxins for hunting SARS-CoV-2 main protease inhibitors: molecular docking, molecular dynamics, pharmacokinetic properties, and reactome study. Pharmaceuticals. 2022;15:153.
[20] Ibrahim MAA, Abdelrahman AHM, Mohamed TA, Atia MAM, Al-Hammady MAM, Abdeljawaad KAA, et al. *In silico* mining of terpenes from red-sea invertebrates for SARS-CoV-2 main protease (m (pro)) inhibitors. Molecules. 2021;26:2082–103.
[21] Case DA, Betz RM, Cerutti DS, Cheatham TE, Darden TA, Duke RE, et al. AMBER. San Francisco: University of California; 2016.
[22] Ibrahim MAA, Abdeljawaad KAA, Abdelrahman AHM, Jaragh-Alhadad LA, Oraby HF, Elkaeed EB, et al. Exploring natural product activity and species source candidates for hunting ABCB1 transporter inhibitors: An *in silico* drug discovery study. Molecules. 2022;27:3104.
[23] Ibrahim MAA, Badr EAA, Abdelrahman AHM, Almansour NM, Shawky AM, Mekhemer GAH, et al. Prospective drug candidates as human multidrug transporter ABCG2 inhibitors: An *in silico* drug discovery study. Cell Biochem Biophys. 2021;79:189–200.
[24] Wang J, Wolf RM, Caldwell JW, Kollman PA, Case DA. Development and testing of a general amber force field. J Comput Chem. 2004;25:1157–74.
[25] Maier JA, Martinez C, Kasavajhala K, Wickstrom L, Hauser KE, Simmerling C. ff14SB: improving the accuracy of protein side chain and backbone parameters from ff99SB. J Chem Theory Comput. 2015;11:3696–713.
[26] Frisch GWT J, Schlegel HB, Scuseria GE, Robb MA, Cheeseman JR, Scalmani G, et al. Gaussian 09, Revision E.01. Wallingford, CT: Gaussian Inc.; 2009.
[27] Bayly CI, Cieplak P, Cornell WD, Kollman PA. A well-behaved electrostatic potential based method using charge restraints for deriving atomic charges - the RESP model. J Phys Chem. 1993;97:10269–80.
[28] Dassault Systèmes BIOVIA. Discovery Studio Visualize, Version 2019. San Diego, CA, USA: Dassault Systèmes; 2019.
[29] Massova I, Kollman PA. Combined molecular mechanical and continuum solvent approach (MM-PBSA/GBSA) to predict ligand binding. Perspect Drug Discov. 2000;18:113–35.
[30] Hou T, Wang J, Li Y, Wang W. Assessing the performance of the molecular mechanics/Poisson Boltzmann surface area and molecular mechanics/generalized Born surface area methods. II. The accuracy of ranking poses generated from docking. J Comput Chem. 2011;32:866–77.
[31] Wang E, Sun H, Wang J, Wang Z, Liu H, Zhang JZH, et al. End-point binding free energy calculation with MM/PBSA and MM/GBSA: Strategies and applications in drug design. Chem Rev. 2019;119:9478–508.
[32] Kim KH, Moon E, Choi SU, Kim SY, Lee KR. Polyphenols from the bark of Rhus verniciflua and their biological evaluation on antitumor and anti-inflammatory activities. Phytochemistry. 2013;92:113–21.
[33] Sikam KG, Happi GM, Ahmed SA, Wakeu BNK, Meikeu LZ, Salau S, et al. *In vitro* antiplasmodial, molecular docking and pharmacokinetics studies of specialized metabolites from *Tetrapleura tetraptera* (Fabaceae). S Afr J Bot. 2022;151:949–59.
[34] Seebacher W, Simic N, Weis R, Saf R, Kunert O. Complete assignments of1H and13C NMR resonances of oleanolic acid, 18? -oleanolic acid, ursolic acid and their 11-oxo derivatives. Magn Reson Chem. 2003;41:636–8.
[35] Bongmo LVL, Nouga AB, Happi GM, Tabekoueng GB, Lateef M, Kamdem Waffo AF, et al. Phytochemical compounds of Guibourtia ehie and their antioxidant, urease and α-glucosidase inhibitory activities. NRFHH. 2022;2:306–12.
[36] Miranda MLD, Garcez FR, Garcez WS. Triterpenes and other constituents from fruits of enterolobium contortisiliquum (Vell.) morong (Fabaceae). Rev Virtual Quim. 2015;7:2597–605.
[37] Kweka Wakeu BN, Talla RM, Jouda J-B, Foudjo Melacheu GL, Muhammad SA, Wandji J, et al. Phytochemical analysis of the stems of Angylocalyx oligophyllus (Baker) Baker f. (Fabaceae). Biochem Syst Ecol. 2022;101:104382.

[38] Ahmadu AA, Delehouze C, Haruna A, Mustapha L, Lawal BA, Udobre A, et al. Betulin, a newly characterized compound in acacia auriculiformis bark, is a multi-target protein kinase inhibitor. Molecules. 2021;26:4599.
[39] Happi GM, Mouthe Kemayou GP, Stammler HG, Neumann B, Ismail M, Kouam SF, et al. Three phragmalin-type limonoids orthoesters and the structure of odoratone isolated from the bark of Entandrophragma candollei (Meliaceae). Phytochemistry. 2021;181:112537.
[40] Honda T, Murae T, Tsuyuki T, Takahashi T. The structure of arjungenin. A new sapogenin from Terminalia arjuna. Chem Pharm Bull. 1976;24:178–80.
[41] Adesina SK, Reisch JA. Triterpenoid glycoside from tetrapleura-tetraptera fruit. Phytochemistry. 1985;24:3003–6.
[42] Jhoo JW, Sang S, He K, Cheng X, Zhu N, Stark RE, et al. Characterization of the triterpene saponins of the roots and rhizomes of blue cohosh (Caulophyllum thalictroides). J Agric Food Chem. 2001;49:5969–74.
[43] An HJ, Kim IT, Park HJ, Kim HM, Choi JH, Lee KT. Tormentic acid, a triterpenoid saponin, isolated from Rosa rugosa, inhibited LPS-induced iNOS, COX-2, and TNF-alpha expression through inactivation of the nuclear factor-kappab pathway in RAW 264.7 macrophages. Int Immunopharmacol. 2011;11:504–10.
[44] Abouelela ME, Orabi MAA, Abdelhamid RA, Abdelkader MSA, Darwish FMM. Chemical and cytotoxic investigation of non-polar extract from ceiba pentandra (L.) gaertn.: a study supported by computer based screening. J Appl Pharm Sci. 2018;8:057–64.
[45] Tsopgni WDT, Happi GM, Stammler HG, Neumann B, Mbobda ASW, Kouam SF, et al. Chemical constituents from the bark of the Cameroonian mahogany Trichilia emetica Vahl (Meliaceae). Phytochem Lett. 2019;33:49–54.
[46] Happi GM, Mbobda ASW, Frese M, Kouam SF, Tchouankeu JC, Lenta BN, et al. A new phenylpropanoid glucoside from Psorospermum tenuifolium Kotschy (Hypericaceae). Trends Phytochem Res. 2021;5:31–6.
[47] Di Pietro ME, Mannu A, Mele A. NMR determination of free fatty acids in vegetable oils. Processes. 2020;8:410.
[48] Gallegos-Infante JA, Rocha-Guzman NE, Gonzalez-Laredo RF, Rico-Martinez R. The kinetics of crystallization of tripalmitin in olive oil: An artificial neural network approach. J Food Lipids. 2002;9:73–86.
[49] Molinier V, Fenet B, Fitremann J, Bouchu A, Queneau Y. Concentration measurements of sucrose and sugar surfactants solutions by using the 1H NMR ERETIC method. Carbohydr Res. 2006;341:1890–5.
[50] Anet FAL, Park J. Proton Chemical-shift assignments in citrate and trimethyl citrate in chiral media. J Am Chem Soc. 1992;114:411–6.
[51] Grindley TB, Szarek WA. Conformational studies on 1,3-dioxepanes. Part IV. applications of geminal coupling constants to conformational analysis of 1,3-dioxepanes. Can J Chem. 1974;52:4062–71.
[52] Martin MT, Rasoanaivo LH, Raharisololalao A. Phenanthridine alkaloids from zanthoxylum madagascariense. Fitoterapia. 2005;76:590–3.
[53] Fuchino H, Kawano M, Mori-Yasumoto K, Sekita S, Satake M, Ishikawa T, et al. *In vitro* leishmanicidal activity of benzophenanthridine alkaloids from Bocconia pearcei and related compounds. Chem Pharm Bull. 2010;58:1047–50.
[54] Yang CH, Cheng MJ, Lee SJ, Yang CW, Chang HS, Chen IS. Secondary metabolites and cytotoxic activities from the stem bark of Zanthoxylum nitidum. Chem Biodivers. 2009;6:846–57.
[55] Wansi JD, Nwozo SO, Mbaze LM, Devkota KP, Donkwe Moladje SM, Fomum ZT, et al. Amides from the stem bark of Fagara macrophylla. Planta Med. 2009;75:517–21.
[56] Cheng MJ, Yang CH, Lin WY, Lin WY, Tsai IL, Chen IS. Chemical constituents from the leaves of Zanthoxylum schinifolium. J Chin Chem Soc. 2002;49:125–8.
[57] Fish F, Meshal IA, Waterman PG. Alkaloids, triterpenes and lignans from the bark of Zanthoxylum dinklagei. Phytochemistry. 1975;14:2094.
[58] Tabekoueng GB, Akak CM, Langat MK, Azebaze AGB, Waffo AFK, Choudhary MI, et al. Chemical constituents from Penianthus camerounensis Dekker (Menispermaceae). Z Naturforsch B. 2019;74:703–8.
[59] Bissim SM, Kenmogne SB, Tcho AT, Lateef M, Ahmed A, Happi EN, et al. Bioactive acridone alkaloids and their derivatives from Citrus aurantium (Rutaceae). Phytochem Lett. 2019;29:148–53.
[60] Ango PY, Kapche DWFG, Kuete V, Ngadjui BT, Bezabih M, Abegaz BM. Chemical constituents of Trilepisium madagascariense (Moraceae) and their antimicrobial activity. Phytochem Lett. 2012;5:524–8.
[61] Paolini J, Wele A, Costa J, Desjobert J-M, Seck M, Fall D, et al. The flavonoid compounds from zanthoxylum leprieurii guill. et perr (rutaceae) extracts and their antioxidant activity against ABTS• +. J Drug Deliv Ther. 2020;10:120–4.
[62] Zazeri G, Povinelli APR, Le Duff CS, Tang B, Cornelio ML, Jones AM. Synthesis and spectroscopic analysis of piperine- and piperlongumine-inspired natural product scaffolds and their molecular docking with IL-1beta and NF-kappaB proteins. Molecules. 2020;25:2841.
[63] Choochana P, Moungjaroen J, Jongkon N, Gritsanapan W, Tangyuenyongwatana P. Development of piperic acid derivatives from Piper nigrum as UV protection agents. Pharm Biol. 2015;53:477–82.
[64] Gomez-Calvario V, Rios MY. (1) H and (13) C NMR data, occurrence, biosynthesis, and biological activity of Piper amides. Magn Reson Chem. 2019;57:994–1070.
[65] Sondengam BL, Kimbu SF, Njimi T, Okogun JI, Ekong DEU. The structure of okolasin, a new alkaloid from Piper guineense. Tetrahedron Lett. 1977;4:367–8.
[66] Acevedo L, Martinez E, Castaneda P, Franzblau S, Timmermann BN, Linares E, et al. New phenylethanoids from Buddleja cordata subsp. cordata. Planta Med. 2000;66:257–61.
[67] Wu L, Li YL, Li SM, Yang XW, Xia JH, Zhou L, et al. Systematic phytochemical investigation of Abies spectabilis. Chem Pharm Bull. 2010;58:1646–9.
[68] McGann M. FRED and HYBRID docking performance on standardized datasets. J Comput Aided Mol Des. 2012;26:897–906.
[69] Mia MM, Hasan M, Miah MM, Hossain MAS, Islam S, Shanta V. Inhibitory potentiality of secondary metabolites extracted from marine fungus target on avian influenza virus-A subtype H5N8 (Neuraminidase) and H5N1 (Nucleoprotein): a rational virtual screening. Vet Anim Sci. 2022;15:100231.
[70] De Vivo M, Masetti M, Bottegoni G, Cavalli A. Role of molecular dynamics and related methods in drug discovery. J Med Chem. 2016;59:4035–61.
[71] Kerrigan JE. Molecular dynamics simulations in drug design. In: Kortagere S, editor. In silico models for drug discovery. Totowa, NJ: Humana Press; 2013. p. 95–113.